Interfacial Microstructural Evolution and Metallurgical Bonding Mechanisms for IN718 Superalloy Joint Produced by Hot Compressive Bonding

JIAN YANG ZHANG, MING YUE SUN, BIN XU, and DIAN ZHONG LI

The novel metallurgical joining process for bonding IN718 superalloy was investigated by hot compressive bonding (HCB) process under the deformation temperature range of 1000 °C to 1150 °C and true strains ranging from 0 to 0.5 at a strain rate of 0.001 s^{-1}. The effect of HCB process parameters on the tensile strength was analyzed. Both the as-deformed and the interfacial microstructures were characterized using the optical microscope, electron backscattered diffraction and transmission electron microscope (TEM) analysis. The results of tensile property revealed that the degree of metallurgical bonding is promoted by increasing deformation temperature and strain. The evolution of the interfacial microstructure showed that the migration of interfacial grain boundary (IGB), which is characterized by discontinuous dynamic recrystallization, is the dominant metallurgical bonding mechanism in the early stages of bonding. TEM analysis indicated that the dislocation density is distributed heterogeneously over both sides of IGB, which is the significant reason for the migration of IGB, during the initial stage of HCB process.

I. INTRODUCTION

THE nickel-based superalloy IN718 is being used in the form of several critical parts of modern aero-engines, gas-turbine components, and extrusion dies.[1–4] These applications require adequate bonding technologies, such as fusion welding (including TIG welding[5]), electron beam welding,[6] diffusion bonding (DB),[7–9] linear friction welding (LFW),[10,11] *etc.*, for joining various components during product application. However, these joining technologies have their inherent disadvantages. For example, when using TIG welding processes, formation of interfacial cracks is still a major problem.[12,13] Other bonding methods, such as DB, commonly require prolonged joining time or complicated heat treatments.[14] Hence, it is of considerable interest to explore a new welding technique which can bond metal joints efficiently with minimal process time.

As a metallurgical bonding technique, hot compressive bonding (HCB) is a process wherein two bonding surfaces initially come into close contact. With the increasing in plastic deformation and temperature, the metal joints are bonded due to the migration of interfacial grain boundary (IGB) by removing the original mating surfaces. The process that controls the kinetics and quality of HCB process is the transformation of the interface into a grain boundary and the subsequent migration of the grain boundary. For successful bonding, the migration of IGB is most beneficial, since it removes imperfections in the interface. HCB is an advanced solid-state joining process and has been applied successfully in steels and superalloys. According to previous research, Gao *et al.*[15] investigated the influences of temperature and strain rate on microstructure and bond strength of the low-carbon steel/high-chromium cast iron bimetal prepared by HCB process. It was found that increasing temperature and reducing strain rate could improve the bond quality due to the increasing elemental diffusion. Sun *et al.*[16] studied the effects of process parameters on the diffusion behaviors of different elements in HCB process of bimetallic samples, and then proposed the element diffusion model considering the influences of different processing parameters. Based on this modified model, the concentration profile and diffusion distance in the transition zone could be well predicted. Yang *et al.*[17] investigated the physical simulation of interfacial microstructural evolution for HCB behavior of

JIAN YANG ZHANG is with School of Materials Science and Engineering, University of Science and Technology of China, Hefei, 230026, P.R. China. MING YUE SUN, BIN XU, and DIAN ZHONG LI are with the Institute of Metal Research, Chinese Academy of Sciences, Shenyang, 110016, P.R. China. Contact e-mail: mysun@imr.ac.cn

GH4169 superalloy. From FEM results, it was found that both the axial and radial mises' stresses have a uniform distribution, and a continuous distribution of mises' stresses in both the axial and the radial directions. The equivalent plastic strain (PEEQ) appeared in the bonding interface. The decreasing extent of the PEEQ along the axial direction is significantly higher than that along the radial direction. Compared with traditional joining methods, such as DB, the significant difference in HCB process is the severe plastic deformation (SPD) on the bonding area. Joining is accomplished through the process of large plastic deformation at elevated temperature. Hence, the crack generated in TIG welding can be resolved with this method. The problems generated in diffusion bonding process, such as long bonding times and lower bonding strength, are also practically solved by means of HCB process. The properties of the materials produced by HCB process can meet the requirements for most critical parts in terms of strength and ductility. For these reasons, the technique is preferred for bonding some superalloys which are used in some critical conditions.

Although as a new metallurgical bonding technique, a few research articles about HCB process have been published in the recent past. However, the effects of the deformation temperature and strain on the bonding behavior of the material are far from being understood. Therefore, this study is conducted with the aim to understand these effects through detailed investigation on the development of bonding area. The evolution of interfacial microstructure under different temperatures and strains was analyzed with optical microscope (OM), electron backscattered diffraction (EBSD), and transmission electron microscope (TEM) methods. The tensile properties of the joints are analyzed. Moreover, the formation mechanism of metallurgical bonding is also discussed in depth.

II. METHODOLOGY

A. Materials

The material used in this study was superalloy (IN718) with the chemical composition as shown in Table I. After solution treatment at 1050 °C for 1 hour, the steels were finally quenched to room temperature in cold water. The initial microstructure with equiaxed grains and annealing twins is shown in Figure 1.

B. Compressive Bonding and Tensile Test

The compression specimens ($\varphi 8$ mm $\times$ 6 mm) were machined from the annealed material. As shown in Figure 2, the contact pair was composed of compression specimens. Before testing, the contact surfaces were polished to remove the oxide, and obtain smooth surfaces. HCB process was conducted in a Gleeble—3500 thermal simulator at the strain rate of 0.001 s^{-1}, in the temperature range of 1000 °C to 1150 °C to attain different true strain levels ranging from 0 to 0.5. In the testing process, all samples were

heated to the temperature with 5 °C s^{-1}, and then held for 5 minutes to eliminate the temperature gradient in each sample. In addition, vacuum level of 2.2×10^{-3} Torr was maintained in the testing chamber. After hot compression tests, the test samples were immediately quenched by cold water.

Tensile test was used to measure the tensile strength of the joints. In order to obtain tensile specimen with HCB joints, two similar round bars, named A and B ($\varphi 10$ mm $\times$ 40 mm) as shown in Figure 3, were hot compressed to weld them together. Then the tensile test samples ($\varphi 8$ mm $\times$ 20 mm) were cut from the bonding joints (A + B). The bonding joints (A + B) were manufactured by HCB using the Gleeble—3500 thermal simulator at the strain rate of 0.001 s^{-1} under the temperature range of 1000 °C to 1150 °C up to the true strain from 0.2 to 0.5. Further, the tensile tests were performed at room temperature on a mechanical testing machine.

C. Microstructure Characterization

The as-deformed samples were cut from the center along with the radial direction in order to examine the interfacial microstructure. The samples containing the interfacial microstructure were grinded and polished by adopting standard procedures. The polished samples were chemically etched in a cupric chloride solution (100 ml HCl + 100 ml CH$_3$CH$_2$OH + 5 g CuCl$_2$). Then the microstructures were investigated by optical microstructure (OM). In order to accurately estimate the recrystallization volume fraction and the mean grain size in the deformed microstructure, the central position of the sample was selected, and seven metallographic images were randomly taken in the vicinity. Then the images were statistically analyzed using Image-J software. EBSD maps were obtained with a step size of 1.0 to 1.5 μm depending on the grain size to be analyzed. For transmission electron microscopy (TEM) observations, the 3-mm diameter disks were machined from the bonding area in a manner that the bonding line runs through the center of the disk along with the radial direction. Then the disks were grinded to 20 μm thickness. Finally, the disks were polished by Ion Beam Grinding machine using double sides of ion beam.

III. RESULTS

A. Microstructure Evolution with Different Compressive Bonding Temperatures

Figure 4 shows the matrix and interfacial microstructural evolution of the samples deformed at different temperatures. It is clear that the bonding interfaces are located in the center of the samples in Figures 4(a), (c), (e), and (g). The statistics of the recrystallization volume fraction and the mean grain size of the samples in Figure 4 are shown in Figure 5. It can be clearly observed from the Figs. that the dynamic recrystallization (DRX) has occurred in the matrix on both sides of the interface. The fraction and size of the recrystallized

Table I.   Chemical Composition (Weight Percentage) of the IN 718

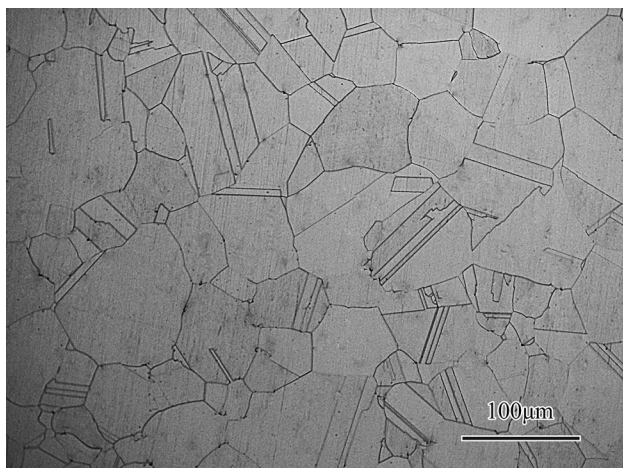| Materials	Ni	Cr	Fe	Nb	Mo	Ti	Al	Co	Si	Mn	Cu	C
IN718	53.35	19.10	17.65	5.18	3.02	0.98	0.56	0.04	0.05	0.03	0.01	0.034

Fig. 1—Initial microstructure of the annealing IN 718.
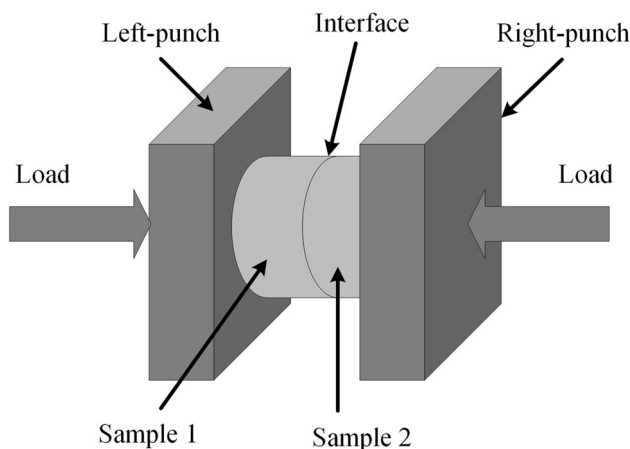
Fig. 2—Sample of HCB process tests.

grains are extremely influenced by the deformation temperature. With a temperature of 1000 °C, a lot of fine equiaxed recrystallized grains are evolved at initial grain boundaries of the mating surfaces. With the increasing temperature, the fraction and size of the recrystallized grain became higher and bigger (Figure 5). It becomes almost fully recrystallized at 1150 °C, while the morphology of the bonding interface at the center of samples significantly varies with the deformation temperatures. It is quite evident from Figure 5 that the bonding interface, shown with the black lines, are becoming more invisible at the centers of all samples. The square regions in Figures 4(a), (c), (e), and (g), including the bonding interface, were magnified by OM, as shown in Figures 4(b), (d), (f), and (h), respectively. It is revealed that the bonding interface gradually

transforms into a curved grain boundary with the increasing deformation temperature. Under relatively low temperature, it can be seen that most sections of the interfacial grain boundary are still straight. With the increasing deformation temperature, some local sections of the interfacial grain boundary, as marked by red dashed line, migrate toward to the opposite side of the interface. When the temperature exceeds 1150 °C, the interface become completely invisible., Above results show that at a given true strain level of 0.5, the straight interface in the center of the deformed samples is gradually replaced by the curved grain boundaries. This phenomenon becomes more prominent with the increasing temperature.

B. Microstructural Evolution with Different True Strains

Figure 6 shows the matrix and interfacial microstructural evolution of the samples deformed to different strains ($0 \leq \varepsilon \leq 0.20$) at the similar deformation temperature (1150 °C) and strain rate (0.001 s^{-1}). When the samples are heated to 1150 °C, many initial interfacial grains, displaying a square-like morphology, are closely arranged on both sides of interface, (Figure 6(a)). It can be observed that the bonding interface in the center of sample is almost completely straight, and there is no possibility of macroscopic void formations at the interface as a result of the polishing process. As shown in Figure 6(b), when the samples are deformed to a true strain of 0.05, the shapes of the initial grains on the interface are gradually transformed into abnormal morphology due to inhomogeneous plastic deformation. In this process, the original smooth grain boundaries are transformed into serrated ones. This phenomenon is commonly regarded as the grain boundary bulging.[18] When true strain is increased to 0.1, many small DRXed grains start to appear on some grain boundaries, and the straight bonding interface is gradually replaced by the curved grain boundaries (as shown by the red dashed lines in Figure 6(c)). This is attributed to the preferential migration of many small interfacial boundaries to the opposite grains during the continuous deformation. When the true strain reaches to 0.2, most of the initial grains are transformed into small DRXed grains. Obviously, the initial straight interface is completely displaced by the curved grain boundaries (as illustrated in Figure 6(d)). The disappearance of the straight interface indicates that the samples are completely bonded by HCB process.

Figure 7 shows the statistics of the mean grain size of the samples, which are deformed to different true strains ($0 \leq \varepsilon \leq 0.50$) by HCB process at 1150 °C. It can be seen from Figure 7 that the mean grain size slightly decreases in the initial stage of the deformation ($\varepsilon = 0.05$), and

then rapidly decreases ($0.05 \leq \varepsilon \leq 0.30$) until it reaches to a steady state ($0.30 \leq \varepsilon \leq 0.50$). It is clear that the coarse-grained starting sample ($D_0 = 230 \ \mu m$) is continuously refined during HCB process until the stable grain size of 45 μm is attained. Taku Sakai[19] attributed such evolution of grains to the mechanism of dynamic recrystallization: the necklace mechanism generally operates from the existing grain boundaries into grain interiors. It is obvious that a typical necklace structure is formed when the deformation strain is 0.10 at 1150 °C, as shown in Figure 6(c). The necklace grain is formed by strain-induced bulging of prior grain boundaries.[20] In addition, it is worth noting that, under the premise of the same initial structure, the mean grain sizes of the deformed structures ($\varepsilon = 0.50$) increase with the increasing deformation temperature (from 1000 °C to 1150 °C), as shown in Figure 5. Obviously, the increasing deformation temperature can accelerate the boundary migration which result in the increased grain growth.

C. Orientation Evolution of Interfacial Microstructures

Figure 8 shows inverse pole figure maps of the interfacial microstructures obtained for different true strains at 1150 °C and at a strain rate of 0.001 s^{-1}, During the primary stage of the compressive bonding ($\varepsilon = 0.05$), the grain boundaries on both sides of the straight bonding interface migrate toward the adjacent ones, as a result of the grain boundary bulging. Several twin grains generate on interfacial grains (as shown in Figure 8(a)). EBSD map shows that the orientations of the initial grains located on each side of bonding

Fig. 4—Matrix and interfacial microstructural evolution results of ▶ the dual samples deformed to strain of 0.5 at a strain rate of 0.001 s^{-1} at different temperatures of (a) 1000 °C, (c) 1050 °C, (e) 1100 °C, and (g) 1150 °C, where (b), (d), (f), and (h) are the magnification of the white square areas in (a), (c), (e), and (g), respectively.

interface are different. With the increasing true strain to 0.10, a large number of small DRXed grains can be observed on both sides of the bonding interface. Twin grains, formed in the initial grains, have all disappeared. In addition, some sections of the bonding interfacial boundaries begin to migrate toward the opposite grains (as shown by white circle in Figure 8(b)). Moreover, the orientation of migrating boundaries remains the same as that of their parent grains. When the true strain is further increased to 0.15, as shown in Figure 8(c), a few new DRXed grains are constantly generated on the bonding interface. Meanwhile, some DRXed grains gradually grow up in size. Clearly, the migrating boundaries generated on the bonding interface continuously migrate in the direction away from the centers of their own curvatures. It is worth noting that the orientations of these migrating boundaries remain the same as those of their own parent grains (as shown by white circle in Figure 8(c)). When the true strain reaches to 0.20, a new grain grows up on the opposite side, such as grain A, shown in Figure 8(d), and the interface finally disappears. From the above results, it is evident that the protrusions of the interfacial grains generated by grain boundary migration always remain in the same orientation as those of their own parent grains during
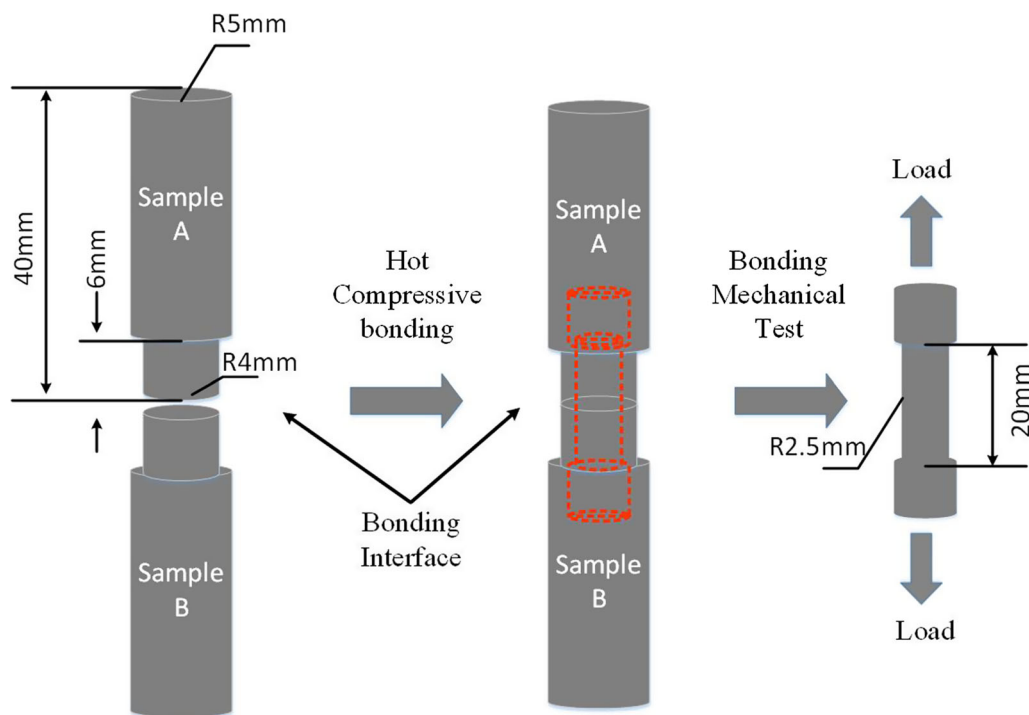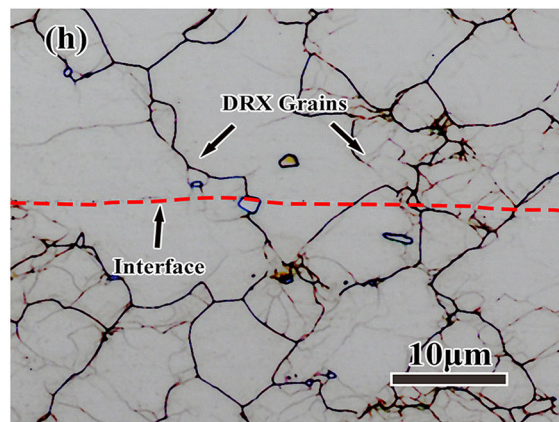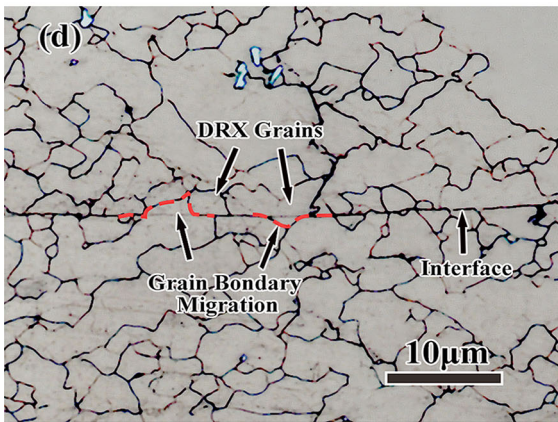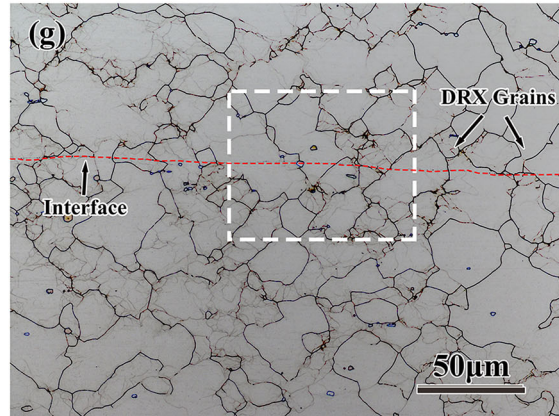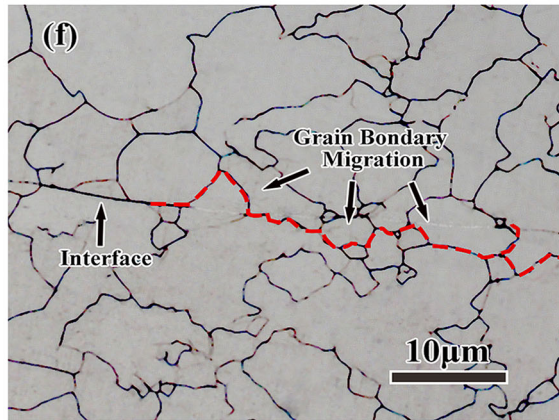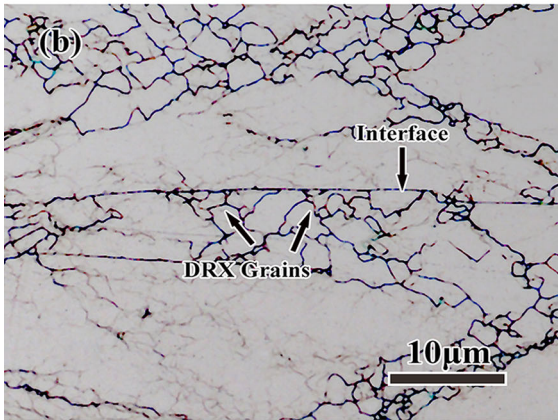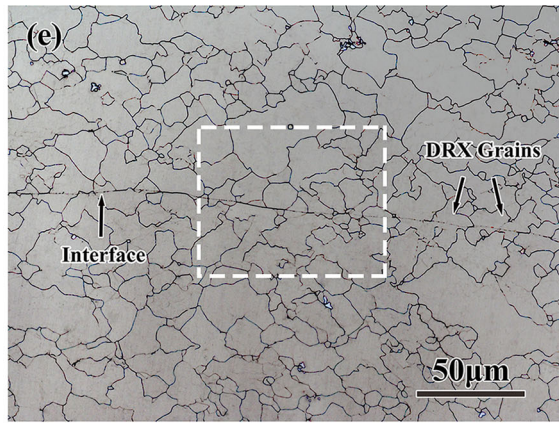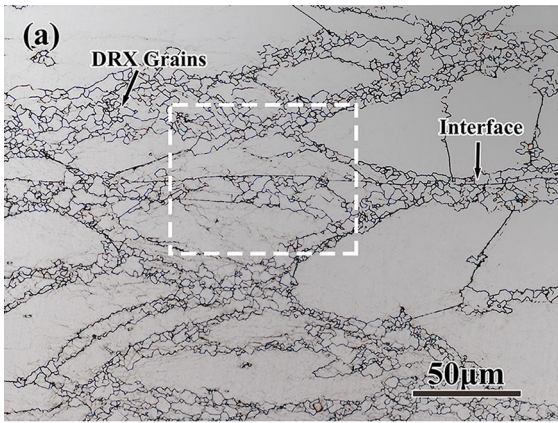

Fig. 3—Schematic of a normal tensile property test process of the HCB-processed sample.
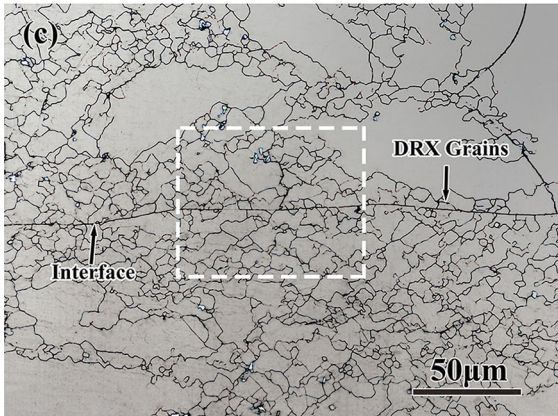
the grain-growth process. In addition, fraction of the low-angle grain boundaries, which is marked by thin-red lines in each grain, does not increase significantly with the increasing strain.
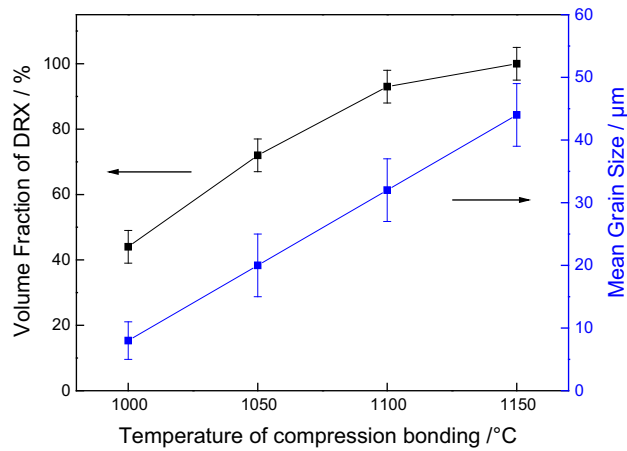
D. *TEM Analysis of Interfacial Microstructures*

Figure 9 shows representative TEM maps of the interfacial microstructures obtained at temperature of 1150 °C with strain rate of 0.001 s^{-1} for different true strain levels. At the beginning of compressive bonding, the interfacial grain boundary maintains a shape of

Fig. 5—Recrystallization volume fractions and mean grain sizes of the samples deformed at different temperatures by HCB process, respectively.
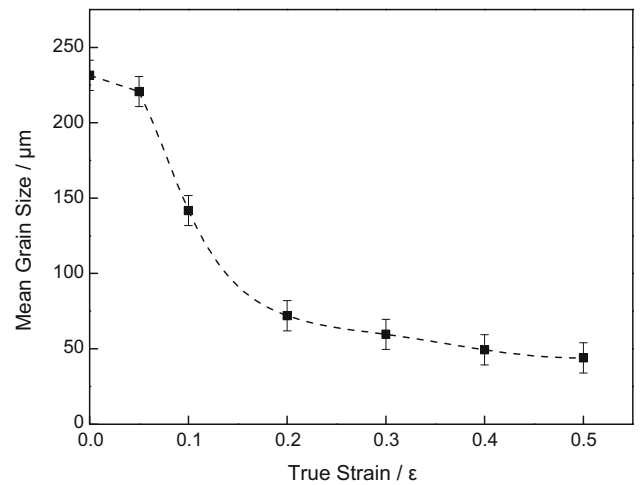

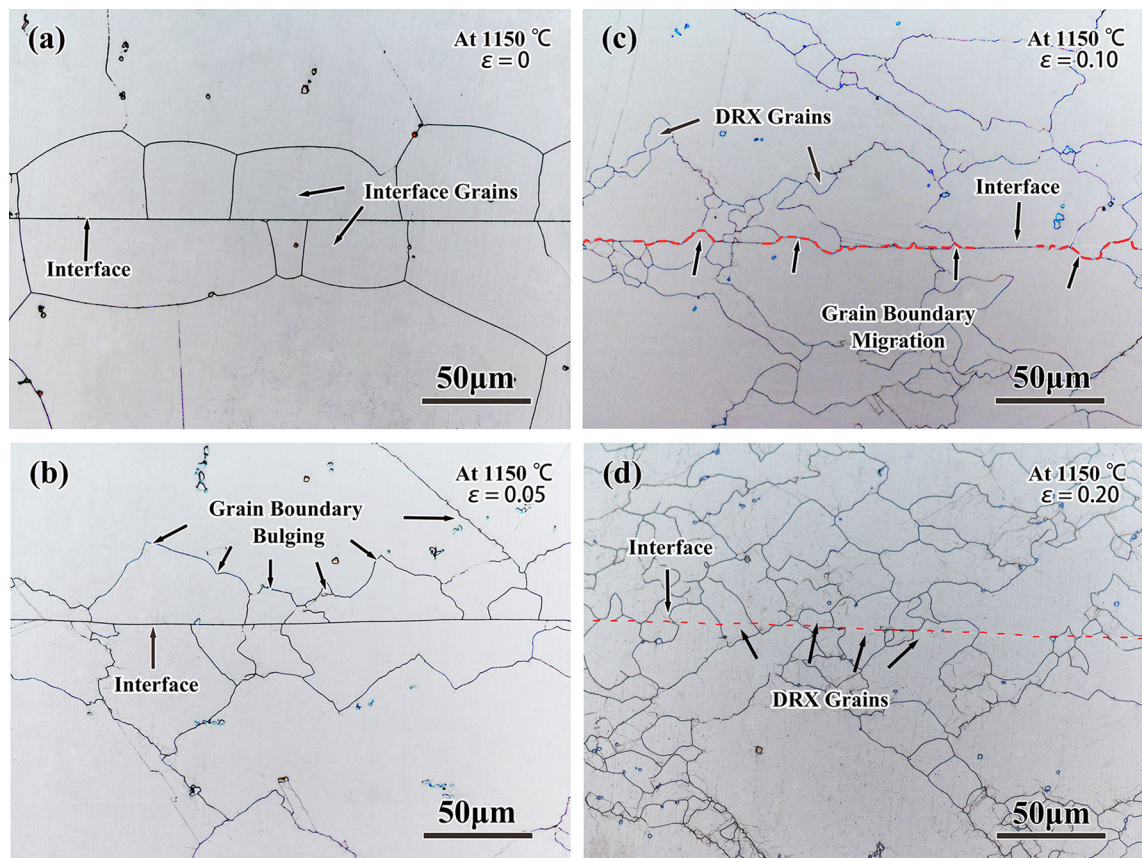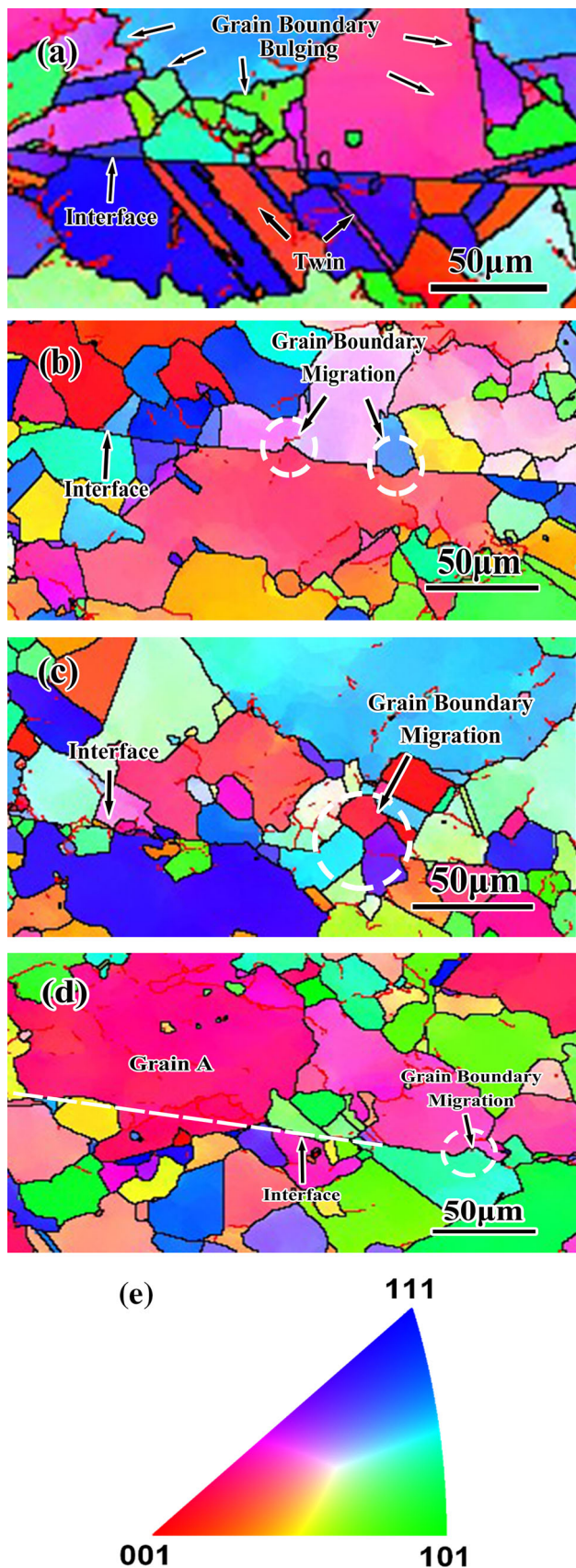Fig. 7—Mean grain sizes of the samples deformed to different true strains at 1150 °C by HCB process.

Fig. 6—Interfacial microstructural evolutions of the samples deformed at temperatures of 1150 °C with strain rates of 0.001 s^{-1} to strain of (*a*) 0, (*b*) 0.05, (*c*) 0.10, (*d*) 0.20.

◄Fig. 8—Inverse pole figure maps of the interfacial microstructures with different strains of (*a*) 0.05, (*b*) 0.10, (*c*) 0.15, (*d*) 0.20, (*e*) color code. (The high-angle grain boundaries and low-angle grain boundaries are indicated by thick-black and thin-red lines, respectively) (Color figure online).

straight line (as shown by dashed white line in Figure 9(a)). Few dislocations are located inside the interfacial grains because of low plastic deformation of the interfacial grains. As the true strain is increased to 0.10, it is clear that a large number of dislocations were generated inside the interfacial grains. Most of them move toward the interfacial grain boundary. Because of the potential activation of different slip systems and the local inhomogeneous plastic deformation, different dislocation densities are observed inside the interfacial grains. It is worth noting that the interfacial grain boundary bulges into the opposite grain, which possesses a higher dislocation density, as shown in Figure 9(b). Upon deformation to a true strain of 0.15, it can be seen that the grain boundary migrates into the opposite side through the initial interfacial grain boundary (marked by yellow arrows in Figure 9(c)). The regions swept by the grain boundary migration have almost no dislocation. When the true strain is further increased to 0.20, the original deformed grains on both sides of interface are all transformed into fully DRXed grains, such as grain A and grain B in Figure 9(d). It appears from Figure 9 that, in the initial stage of deformation ($0 \leq \varepsilon \leq 0.10$), the number of dislocations in the interfacial grains gradually increases with the increasing true strain. Subsequently, most of them move to the grain boundaries, resulting in the increasing dislocation density at the grain boundaries. It is known that the dislocation storage rate may be dependent on grain orientation during the deformation process.[21] Hence, the dislocation densities on both sides of the interface are in contrast to each other. It can be observed that the grain boundary migrates from one side (with a lower dislocation density) to the other side, having a higher number of dislocations. The effect of this migration is to reduce the total number of dislocations in the deformed sample. The TEM observations are in complete agreement with the OM and EBSD results.

E. *Mechanical Property*

The effects of deformation temperature and true strain on the strength and elongation of the bonding joints are shown in Figure 10. It is obvious that the yield strength, tensile strength, and elongation increase with the increasing deformation temperature and true strain (Figures 10(c) and (d)). Combined with the evolution of microstructure, it is easy to understand that the lowest strength and elongation in Figure 10(c) are attributable to no migration in IGB (Figures 4(a) and (b)). It is worth noting that the increasing grain size leads to a decrease in strength and ductility for metals. However, with the increasing deformation temperature
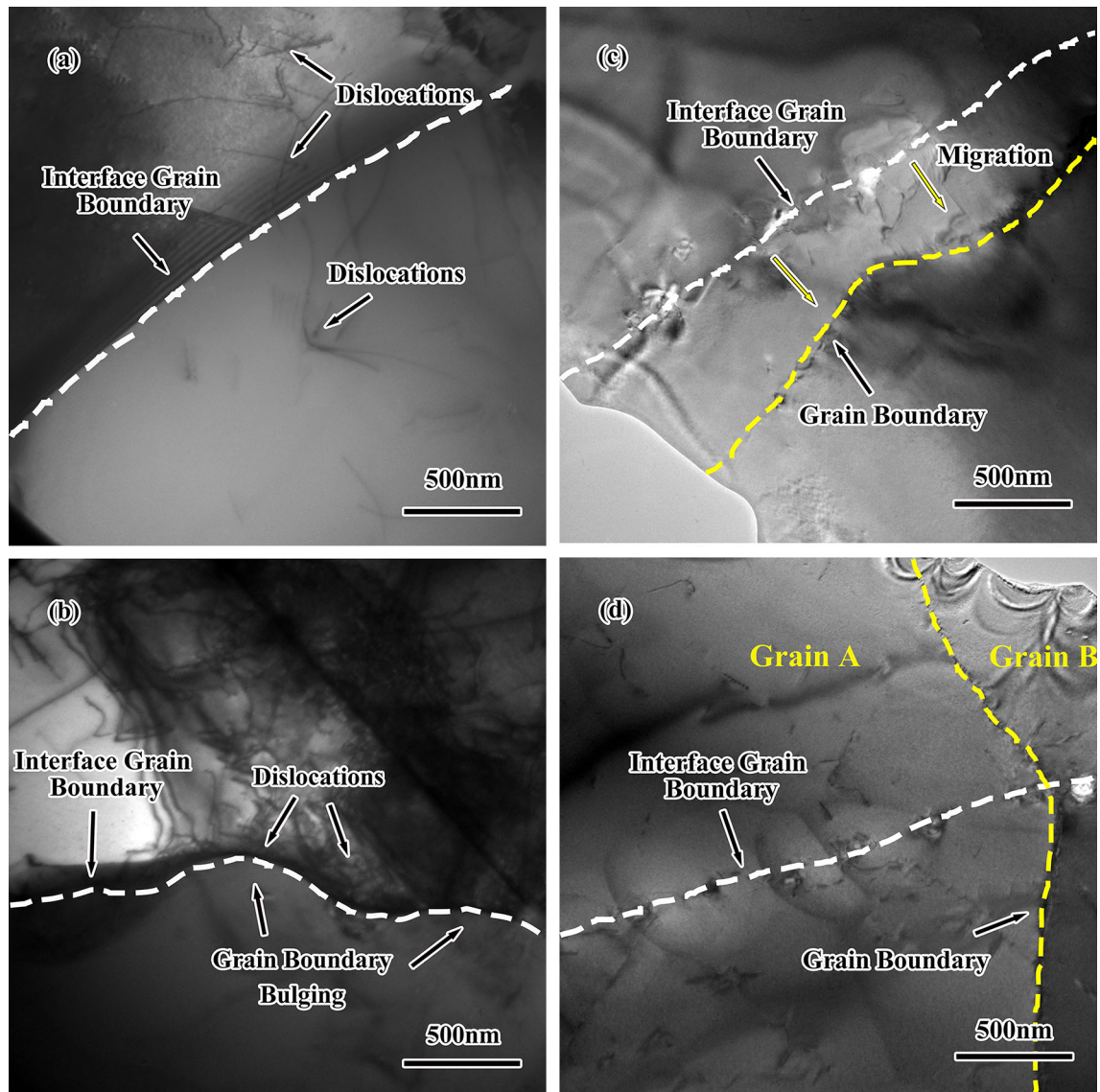
Fig. 9—TEM maps of the interfacial microstructures showing the interfacial grain boundary migrations obtained at temperature of 1150 °C at strain rates of 0.001 s^{-1} to strains of (a) 0.05, (b) 0.10, (c) 0.15, (d) 0.20.

from 1050 °C to 1150 °C, the strength has not decreased, so much so the plasticity is increased, since the grain growth was observed in the bonded joints (Figure 5). Obviously, the migration in IGB plays a crucial role in enhancing strength and ductility of the bonded joints. The increased strength and ductility of HCB sample (Figure 10(d)), not only result from the refined grains (Figure 7), but also arise from more complete migration of IGB. The interfacial grains grow across the bonding interface by IGB migration, and the crack growth though these grains becomes not facility, thus leading to the stronger joints.[22] It is evident that the migration of the IGB is a necessary morphological characteristic of high-quality bonding with good performance under various testing conditions.

IV. ANALYSIS AND DISCUSSION

A. Interfacial Microstructural Evolution

Evidences from the matrix and interfacial microstructure, as well as the EBSD and TEM analysis, suggest that the following processes had occurred during HCB process. The microstructures of the bonding interface in the center of sample do significantly vary with the compressive bonding temperatures. With the increasing deformation temperature, the bonding interfaces are becoming more invisible in the centers of all the samples. That is because the straight interface in the center of the deformed sample is increasingly replaced by the curved grain boundaries with the increasing deformation temperature.
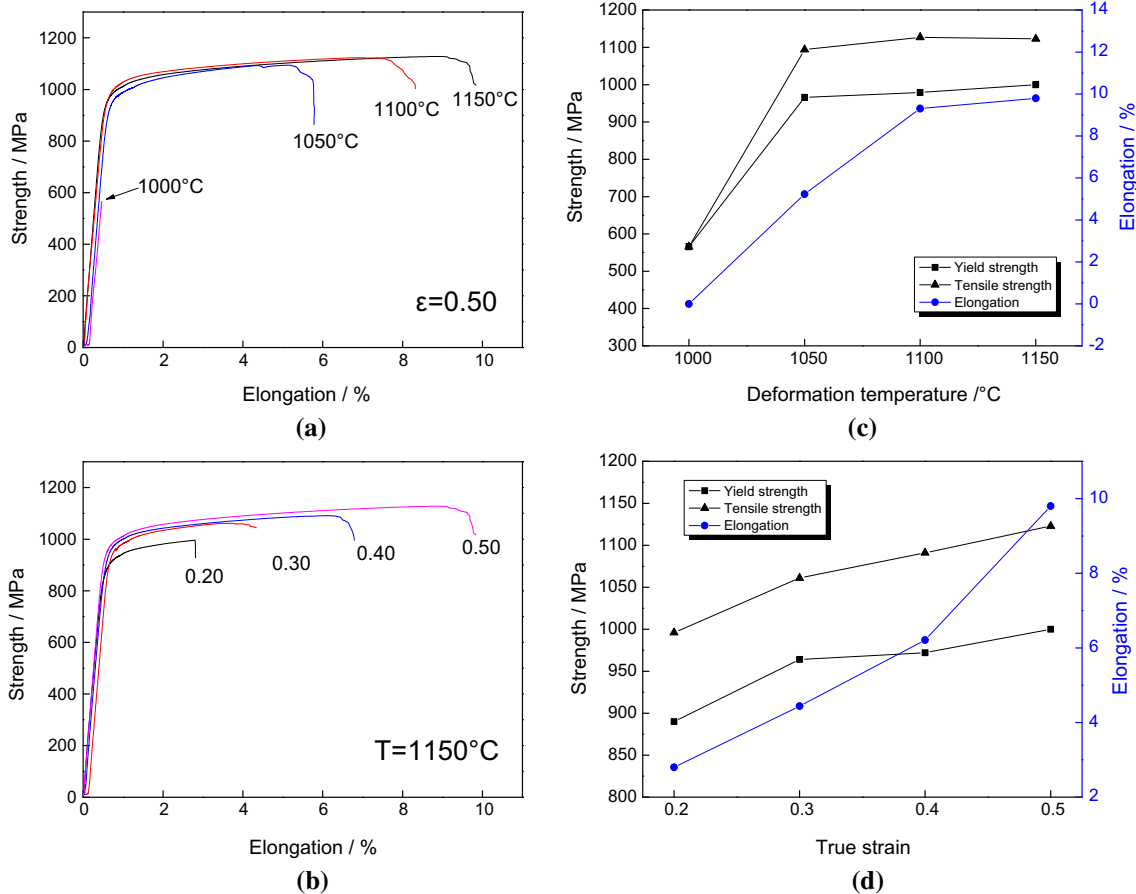
Fig. 10—Tensile curves of the joints bonded at different temperatures (*a*) and true strains (*b*); and the temperature and strain dependences of strength and elongation (*c*) and (*d*), respectively.

When the compressive bonding tests are conducted at 1150 °C, it can be observed that DRX grains are first generated on the matrix grain boundaries, and then many small portions of the grain boundaries on the bonding interface gradually migrate into the opposite grains and finally become curved ones with the increasing true strain, resulting in the complete disappearance of the straight bonding interface. EBSD analysis shows that the protrusions of the interfacial grains generated by grain boundary migration have the similar orientation to that of their own parent grains. Further investigation by TEM shows that the number of dislocations in the interfacial grains gradually increases with the increasing true strain. The interfacial grain boundaries migrate towards the adjacent grains, having a higher of dislocation density.

B. *Compressive Bonding Mechanism*

The observations of interfacial microstructures clearly indicate that the migration of grain boundary occurred on the bonding interface during compressive bonding process of IN718 superalloy. This phenomenon also appeared in the DB process. Few mechanisms of interfacial migration have been proposed by many researchers, such as Kirkendall effect being applied to

dissimilar DB of materials,[23] and concentration gradient effect existing in transient liquid-phase diffusion bonding process.[24] However, these mechanisms are not applicable to hot compressive deformation bonding, because Kirkendall effect or concentration gradient effect only exists between dissimilar materials.

During this compressive bonding of similar materials, it was revealed that the evolution of interfacial grains takes place in two stages: the first stage is the DRX process which occurs in the initial grains as a fall-out of the previous deformation operation. The second stage is the metallurgical bonding process in which small grain boundaries on the interface first bulge into the opposite side, and then the bulging boundaries continue to migrate with the increasing strain. Hence, it seems that the mechanism of interfacial grain boundary migration is probably related to DRX of interfacial grains.

It is well known that the nucleation mechanisms associated with dynamic recrystallization can be classified as two types: *i.e.,* discontinuous dynamic recrystallization (DDRX) and continuous dynamic recrystallization (CDRX).[25,26] The DDRX is characterized by nucleation of new grains through grain boundary bulging phenomenon followed by growth of the recrystallized grains.[27,28] On the contrary, CDRX commonly involves the formation of low-angle grain

boundaries (LAGBs), which transform to high-angle grain boundaries (HAGBs), with the increasing misorientations of the subgrain boundaries.[29] Obviously, there is no nucleation in CDRX.

In Figure 8, according to the EBSD map, it is quite clear that under relatively small strains, the grain boundaries are completely bulged. These bulged regions may act as potential sites for the subsequent nucleation of DRX through the migration of grain boundaries. This indicates that DDRX, characterized by nucleation through grain boundary bulging, is the primary mechanism of DRX for IN718 during HCB process. It is also found that some parts of the IGB bulge into the opposite grains during the initial stage of DRX. The grain orientations of the bulged regions on the interface remain the same as that of their own parent grains (white circles in Figures 8(b), (c) and (d)). It is demonstrated that the bulging of interfacial grain boundaries results in metallurgical bonding of the interface. Therefore, the interfacial grain boundary bulging, which is characterized by DDRX, is the dominant metallurgical bonding mechanism in the early stage of bonding.

In general, grain boundary bulging is driven by the energy difference between the adjacent grains.[30] The TEM analysis of the interfacial microstructure in Figure 9 revealed that the nonuniform deformation of interfacial grains at the initial stage of HCB process could give rise to the difference of the dislocation densities on opposite sides of IGB. This would cause the difference of distortion energies in the location of IGB. Subsequently, a small portion of IGB bulges from the lower distortion energy level to the higher one. Compared with the grains in the matrix, the occurrence of bulging on the IGB is invariably delayed. This is due to the fact that the straight boundary needs more energy to move than the curved one.

V. CONCLUSIONS

The interfacial microstructural evolution of IN718 superalloy was investigated by HCB process tests. The metallurgical bonding mechanisms of the interface were analyzed. The main conclusions drawn from this work are the following:

1. As the deformation temperature increases, a higher fraction of bigger recrystallized grains appears in the matrix structure, and the bonding interface becomes more invisible.
2. The interfacial microstructural evolution includes two stages during HCB process. The first stage is the DRX process that occurs on the initial grain boundaries at the beginning of deformation. DDRX, characterized by nucleation through grain boundary bulging, is the primary mechanism of DRX for IN718 during HCB process at 1150 °C with small strain. The second stage is the metallurgical bonding process, in which a small portion of IGB first bulges into the opposite side, and then the bulging IGB continues to migrate with the increasing strain. The migration of IGB is the domi-

nant metallurgical bonding mechanism in the early stage of HCB process.
3. The nonuniform deformation of interfacial grains at the initial stage of HCB process readily results in the difference of dislocation densities on opposite sides of IGB. On the other hand, the driving force for IGB migration is the energy difference, which is caused by the difference in the numbers of dislocation densities on the opposite sides of IGB.
4. The strength and elongation both increase with the increasing deformation temperature and true strain. The migration of IGB is a necessary morphological characteristic of high-quality bonding with good performance corresponding to that of the tensile test results under different conditions.

REFERENCES

1. D. Furrer and H. Fecht: *JOM*., 1999, vol. 51, pp. 14–17.
2. D. Locq and P. Caron: *J. Aerosp. Lab*, 2011, vol. 3, p. 1.
3. A. Mugarra, K. Ostolaza, and J.L. Alcaraz: *J. Mater. Process. Technol.*, 2002, vols. 125–126, pp. 549–54.
4. R.E. Schafrik, D.D. Ward, and J.R. Groh: *Superalloys*, 2001, vol. 1, pp. 1–11.
5. K.D. Ramkumar, B.M. Kumar, M.G. Krishnan, S. Dev, A.J. Bhalodi, N. Arivazhagan, and S. Narayanan: *Mater. Sci. Eng. A*, 2015, vol. 639, pp. 234–44.
6. S.K. Sharma, P. Agarwal, and J.D. Majumdar: *Procedia Manuf.*, 2016, vol. 7, pp. 654–59.
7. W.B. Han, K.F. Zhang, B. Wang, and D.Z. Wu: *Acta Metall Sin.*, 2007, vol. 20, pp. 307–12.
8. A.A. Shirzadi and E.R. Wallach: *Sci. Tech. Weld. Join.*, 2013, vol. 9, pp. 37–40.
9. G. Zhang, R.S. Chandel, and H.P. Seow: *Sci. Tech. Weld. Join.*, 2001, vol. 6, pp. 235–39.
10. T.J. Ma, X. Chen, W.Y. Li, X.W. Yang, Y. Zhang, and S.Q. Yang: *Mater. Des.*, 2016, vol. 89, pp. 85–93.
11. R. Damodaram, S.G.S. Raman, D.V.V. Satyanarayana, G.M. Reddy, and K.P. Rao: *Mater. Sci. Eng. A*, 2014, vol. 612, pp. 414–22.
12. I. Woo, K. Nishimoto, K. Tanaka, and M. Shirai: *Weld. Int.*, 2000, vol. 14, pp. 365–74.
13. H. Kuroki: *Weld. Int.*, 1999, vol. 13, pp. 945–51.
14. I. Sah, D. Kim, H.J. Lee, and C. Jang: *Mater. Des.*, 2013, vol. 47, pp. 581–89.
15. X. Gao, Z. Jiang, D. Wei, S. Jiao, D. Chen, J. Xu, X. Zhang, and D. Gong: *Mater. Des.*, 2014, vol. 63, pp. 650–57.
16. C. Sun, L. Li, M. Fu, and Q. Zhou: *Mater. Des.*, 2016, vol. 94, pp. 433–43.
17. X. Yang, W. Li, Y. Feng, S. Yu, and B. Xiao: *Mater. Des.*, 2016, vol. 104, pp. 436–52.
18. X.P. Wei, W.J. Zheng, Z.G. Song, T. Lei, Q.L. Yong, and Q.C. Xie: *J. Wuhan Univ. Technol.*, 2014, vol. 29, pp. 379–83.
19. T. Sakai: *J Mater. Process. Technol.*, 1995, vol. 53, pp. 349–61.
20. D. Ponge and G. Gottstein: *Acta Mater.*, 1998, vol. 46, pp. 69–80.
21. I.L. Dillamore and H. Katoh: *Metal Sci.*, 1974, vol. 8, pp. 73–83.
22. C. Zhang, H. Li, and M.Q. Li: *Sci. Technol. Weld. Join.*, 2015, vol. 20, pp. 115–22.
23. B. Alemán, L. Gutiérrez, and J.J. Urcola: *J. Mater. Sci. Technol.*, 2013, vol. 9, pp. 633–41.

24. Y. Zhou, W.F. Gale, and T.H. North: *Int. Mater. Rev.*, 1995, vol. 40, pp. 181–96.
25. H.J. McQueen: *Mater. Sci. Eng. A*, 2004, vol. 387, pp. 203–08.
26. S.M.F. Varzaneh, A.Z. Hanzaki, J.M. Cabrera, and P.R. Calvillo: *Mater. Chem. Phys.*, 2015, vol. 149, pp. 339–43.
27. Z. Yanushkevich, A. Belyakov, and R. Kaibyshev: *Acta Mater.*, 2015, vol. 82, pp. 244–54.
28. M.G. Jiang, H. Yan, and R.S. Chen: *J. Alloy. Compd.*, 2015, vol. 650, pp. 399–409.
29. T. Sakai, H. Miura, A. Goloborodko, and O. Sitdikov: *Acta Mater.*, 2009, vol. 57, pp. 153–62.
30. H.S. Lee, J.H. Yoon, and W.H. Cho: *Adv. Mater. Res.*, 2011, vols. 228–229, pp. 666–71.